ARTICLE

UV Photolysis of N_2O Isotopomers: Isotopic Fractionations and Product Rotational Quantum State Distributions

Mohammad Noh Daud*

Department of Chemistry, University of Malaya, Kuala Lumpur 50603, Malaysia

(Dated: Received on April 12, 2011; Accepted on October 31, 2011)

The time-dependent quantum wave packet method is used to study the dynamics of the photodissociation processes for the isotopomers $^{14}N^{14}N^{16}O$, $^{14}N^{15}N^{16}O$, $^{15}N^{14}N^{16}O$, $^{15}N^{15}N^{16}O$, $^{14}N^{14}N^{17}O$, and $^{14}N^{14}N^{18}O$. In general, the computed isotopic fractionation factors derived from the absorption cross sections of five heavy isotopomers are in good agreement with the experimental results. Relative to the $^{14}N^{14}N^{16}O$ isotopomer, the N_2 rotational state distributions for the isotopically nitrogen substituted N_2O are found to be entirely shifted to higher rotational states. Similar to its isotopic fractionation factors, the N_2 rotational state distributions for the asymmetric isotopomers $^{14}N^{15}N^{16}O$ and $^{15}N^{14}N^{16}O$ are found to be observably different.

Key words: Time-dependent wavepacket, Isotopic fractionation, Product rotational distribution

I. INTRODUCTION

Nitrous oxide (N_2O) actively absorbs infrared radiation in the atmosphere and thereby contributes to greenhouse warming. It is emitted into the atmosphere from natural and anthropogenic sources including the oceans, soil, biomass burning, the combustion of fuels, catalytic converters for automobiles and various industrial processes [1]. It is removed from the atmosphere mainly by photolysis in the stratosphere. The bulk of the N_2O photolysis occurs on the shoulder of its absorption profile at ultraviolet wavelengths around 200 nm, between the Schumann-Runge bands and Herzberg continuum of O_2 absorption, rather than at the peak of the absorption band [1−3].

$$N_2O(X^1\Sigma^+) + h\nu \rightarrow N_2(X^1\Sigma_g^+) + O(^1D)$$

The discovery in the isotopic fractionation of heavy stratospheric N_2O in various processes suggests the process preferentially destroys light oxygen and nitrogen isotopes [2−12], where the photolytic fractionation factor is defined as the ratio of the heavy to light spectrum, $\epsilon=(\sigma_{\rm heavy}/\sigma_{\rm light}-1)10^3$. In an effort to explain the heavy stratospheric N_2O, Yung and Miller suggested that the difference in the zero point vibrational energy for the heavier N_2O isotopomers causes a blue-shift in the ultraviolet spectrum, resulting in fractionation during ultraviolet photolysis [13].

Due to the importance of N_2O in atmospheric chemistry, its photodissociation processes has been the focus of several theoretical investigations [14−19]. A deeper understanding of the electronic excitations is provided by the theoretical work of Daud *et al.* [15], who performed extensive multireference configuration interaction (MRCI) calculations for the energies of the six lowest electronic states and the transition dipole moments connecting the ground state to the excited electronic states. The first absorption band of N_2O in the ultraviolet region is mainly due to the transitions to $^1\Sigma^-$ and $^1\Delta$ states, for which three upper states, the $^1A'$ and $^1A''$ Renner-Teller components of $^1\Delta$ and $^1A''(^1\Sigma^-)$ are expected. The dissociation proceeds via a conical intersection with the repulsive $^1A'(^1\Pi)$ and $^1A''(^1\Pi)$ states, which correlates with $N_2(X^1\Sigma_g^+)$+$O(^1D)$ products. Dipole transitions from the ground $^1\Sigma^+$ state to the excited $^1\Sigma^-$ and $^1\Delta$ states are forbidden in the collinear geometry, but weakly allowed for bent geometries. Because the two bent states are involved in the dissociation, much of the available energy is channeled into rotational motion of N_2.

In this work, an extensive study of the photodissociation dynamics of N_2O in its first absorption band (between 150 and 210 nm) for several N_2O isotopomers was carried out. The calculations for product state distributions of several isotopomers of N_2O are presented. Employing the constructed absorption spectra, the wavelength- and temperature-dependent isotopic fractionation factors are determined and compared with the experimental observations.

II. THEORY

The dynamics computations were based on the N_2O potential energy surfaces (X^1A', $1^1A''$, $2^1A'$ and $2^1A''$)

*Author to whom correspondence should be addressed. E-mail: mnoh@um.edu.my

constructed previously using the multireference configuration interaction approach [15]. Employing the computed ground state X^1A' wave functions, and the corresponding transition dipole moments connecting the ground state, X^1A', to the three excited states, $1^1A''$, $2^1A'$ and $2^1A''$, the initial wavepackets were constructed. Then the wavepackets were propagated with time until it reached the defined asymptotic region of the potential energy surfaces. In the present work the N−NO internuclear distance is fixed at its equilibrium geometry, 2.13199 bohr based on the fact that the experiments have shown that the N_2 products are produced vibrationally cold with the amount of v=1 less than 2% of the v=0 products. All the computations are performed on a uniform computational grid in which 64 angular grid and 384 radial grid points have been used. The time-dependent quantum wave packet method is used to calculate the total absorption cross section from the photodissociation of N_2O. Details of the photodissociation theory of absorption cross section have been described elsewhere [20−24].

The partial cross section to yield specific product rotational states is obtained from an analysis line method at large inter-fragment separation introduced by Balint-Kurti *et al.* [20, 21, 25]. The partial photofragmentation cross section for the production of a particular diatomic vibrational-rotational state at any energy can be calculated from the half Fourier transform of the coefficient of an asymptotic analysis of the wave packet at each time step [20, 21, 25]:

$$\sigma_j(J,K,E) = \frac{4\pi^3\nu k_j}{3c\epsilon_0\mu}\left|A_j^{J,K}(R=R_\infty,E)\right|^2 \quad (1)$$

$$A_j^{J,K}(R=R_\infty,E) = \frac{1}{2\pi}\int_{t=0}^{\infty}\exp\left(\frac{iEt}{\hbar}\right)\cdot C_j^{J,K}(R=R_\infty,t)\,\mathrm{d}t \quad (2)$$

here J is the total angular momentum quantum number, K is the projection of the angular momentum quantum number of the total angular momentum vector **J** on the N_2−O internal axis R and $C_j^{J,K}(R{=}R_\infty,t)$ is an expansion coefficient for a product state wave function

$$\Phi^{J,K}(r,R=R_\infty,\theta,t) = \sum_j C_j^{J,K}(R=R_\infty,t)\cdot \Theta_{jK}(\theta)\,\chi_j(r) \quad (3)$$

where χ_j is the vibrational wave functions, and Θ_{jK} is the rotational wave functions of normalised associated Legendre polynomials. The expansion coefficients are then obtained from

$$C_j^{J,K}(R=R_\infty,t) = \left\langle \Theta_{jK}(\theta)\,\chi_j(r)\right|\cdot \sum_K \Phi^{J,K}(r,R=R_\infty,\theta,t)\Big\rangle \quad (4)$$

where R_∞ is located in the asymptotic region of the potential.

An analysis plane was located at a N_2−O separation of 11.34 bohr, corresponding to the radial grid point at 311 out of 384 points. At each time step, a cut was taken through the wave packet along this plane and the resulting two-dimensional wave function was analyzed into its fragment state distribution. The exchange symmetry of the same two N nuclei was employed and this means that 64 Gauss-Legendre angular quadrature points allow us to represent N_2 rotational wave functions with rotational quantum number j up to 127.

The outgoing wave packet is absorbed beyond the $R{=}R_\infty$ line to prevent reflection at the edge of the finite grid using a negative imaginary damping potential of a cubic form [26, 27].

$$V_{\mathrm{damp}}(R) = \begin{cases} 0.0, & R < R_{\mathrm{damp}} \\ -iA_{\mathrm{damp}}\left(\dfrac{R-R_{\mathrm{damp}}}{R_{\mathrm{max}}-R_{\mathrm{damp}}}\right)^3, & R_{\mathrm{damp}} \leq R \leq R_{\mathrm{max}} \end{cases} \quad (5)$$

where R_{damp} is the point at which the damping is "switched on" and A_{damp} is an optimized parameter giving the strength of the damping. The total propagation time required for the wave function to leave the interaction region was approximately 10.24 ps, with the time step used for the propagation being 10 fs. The damping was switched on at 356 out of 384 points, while the dimensionless parameter A_{damp} has been previously optimized by Vibók and Balint-Kurti [26, 27] to be set as 0.1014.

III. RESULTS AND DISCUSSION

A. Isotopic fractionation factors

In the present work, the theoretical fractionation factors were computed as a function of wavelength based on the constructed absorption cross sections (reader may need to refer Ref.[5] for further explanation regarding with the computed cross section). In Fig.1−Fig.4, the wavelength-dependence of the isotopic fractionation factors experimentally observed by several workers is compared with the computed results. Isotopic fractionation derived data by Hessberg *et al.* [11] from ultraviolet spectroscopic measurements of $^{14}N^{14}N^{16}O$, $^{15}N^{14}N^{16}O$, $^{14}N^{15}N^{16}O$, and $^{15}N^{15}N^{16}O$ at 233 and 283 K serve as a very good comparison with our theoretical predictions. The fractionation is calculated from the ratio of the intensity of the ultraviolet spectrum between two different isotopomers. Qualitatively, our predictions appear to be very well between 195 and 220 nm with the largest discrepancies coming from the $^{14}N^{15}N^{16}O$ isotopomer at 233 K. At shorter wavelengths between 170 and 195 nm, there are significant discrepancies between the theory and experiment. A

DOI:10.1088/1674-0068/24/06/679-685

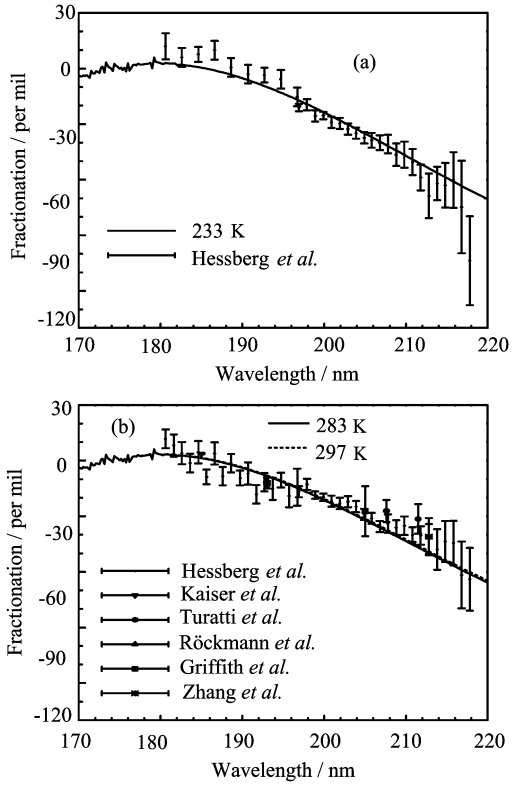

FIG. 1 Theoretical and experimentally measured isotopic fractionation factors for the $^{15}N^{14}N^{16}O$ isotopomer photolysis at several different temperatures. (a) T=233 K, (b) T=283 K, and $T\approx$297 K. Experimental values were taken from Griffith *et al.* [5], Kaiser *et al.* [7], Röckmann *et al.* [9], Turatti *et al.* [10], von Hessberg *et al.* [11], Zhang *et al.* [12].

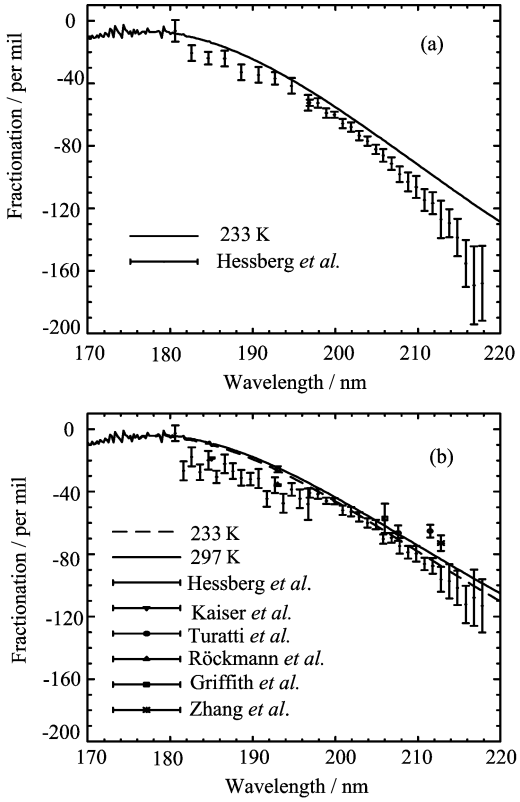

FIG. 2 Theoretical and experimentally measured isotopic fractionation factors for the $^{14}N^{15}N^{16}O$ isotopomer photolysis at several different temperatures: (a) T=233 K, (b) T=283 K, and $T\approx$297 K. Experimental values were taken from Griffith *et al.* [5], Kaiser *et al.* [7], Röckmann *et al.* [9], Turatti *et al.* [11], von Hessberg *et al.* [11], Zhang *et al.* [12].

possible source of the disagreement could be the failure of the theory to correctly predict the oscillatory structures observed in the experimental spectra. Note that the intensity of the $^{14}N^{14}N^{16}O$ absorption spectrum in the banded region has also displayed some disagreements between several independent experiments and it seems very difficult to get reliable results around the maximum peak [28−32]. Very interestingly, the experimental result for the $^{15}N^{14}N^{16}O$ isotopomer is consistent with our current prediction of positive fractionation around the absorption peak between 180 and 186 nm, particularly at 233 K. Included in Fig.1(b) and Fig.2(b) as well are the results of other experimental measurements at ambient temperature, displaying a quite good agreement with theory.

Our results of the $^{14}N^{14}N^{18}O$ isotopomer are in reasonable agreement with the experimental values as displayed in Fig.4(b). The fractionation factor at the absorption maximum at 182 nm observed by Kaiser *et al.* displays a positive value while ours is negative [7]. Larger errors in the fractionation factor measured by Griffith *et al.* is due to temperature variation of stratospheric samples [5]. Isotopic fractionation of N_2O is sensitive to temperature variation, so it is not surprising that some discrepancies can be observed between the experimental measurements. Also displayed is the prediction of the isotopic fractionation factors for the $^{14}N^{14}N^{17}O$ isotopomer as in Fig.4(a).

The larger negative value at longer wavelengths indicates that the N_2O molecule in the atmosphere will be dominated by absorption in the low-energy tails (between 195 and 210 nm) and the substitution fractionations corresponding to these absorptions. In general, both theoretical predictions and experimental data qualitatively agree on increasingly negative fractionation factors at longer wavelengths in the order of $^{15}N^{15}N^{16}O$>$^{14}N^{15}N^{16}O$>$^{14}N^{14}N^{18}O$ >$^{15}N^{14}N^{16}O$>$^{14}N^{14}N^{17}O$. We have seen that the isotopic fractionation factors calculated from the time-dependent method reproduce the experimental fractionation factors for photon energies above 195 nm remarkably well. The major contributor of fractionation in these energies region is due to the different populations of hot band excitations of the various heavier isotopomers. Therefore, the general concept of fractionation being caused by spectral shifts induced by iso-

DOI:10.1088/1674-0068/24/06/679-685

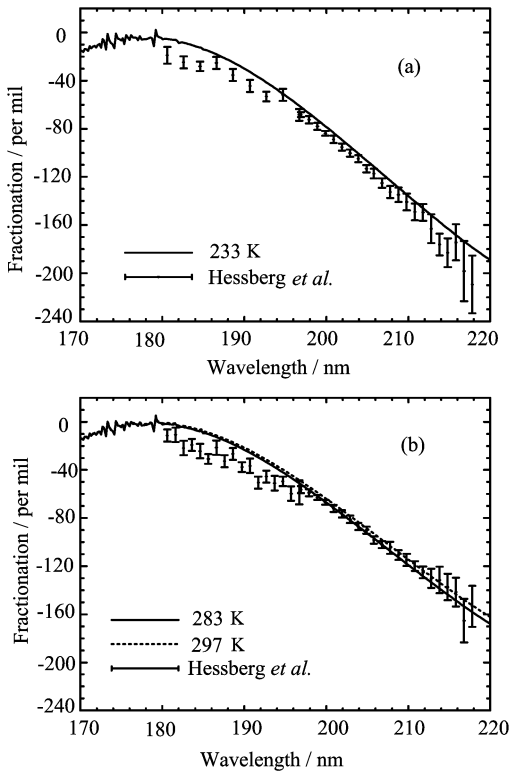

FIG. 3 Theoretical and experimentally measured isotopic fractionation factors for the $^{15}N^{15}N^{16}O$ isotopomer photolysis at several different temperatures: (a) T=233 K, (b) T=283 K. Experimental values were taken from Hessberg *et al.* [11].

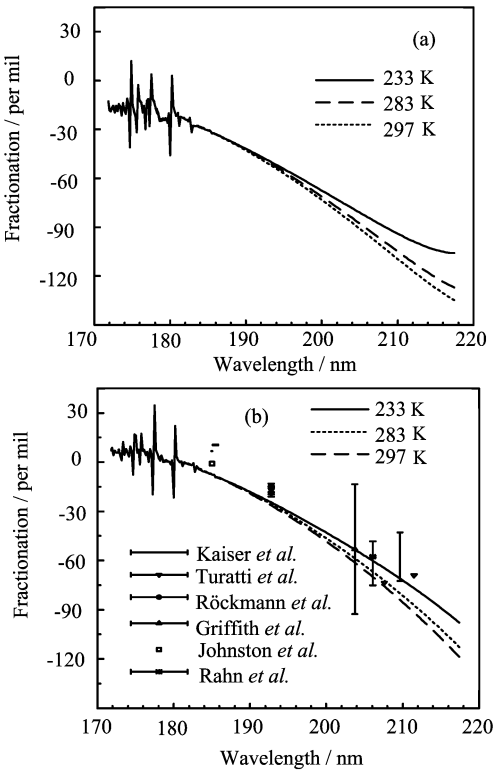

FIG. 4 (a) Theoretical isotopic fractionation factors for the $^{14}N^{14}N^{17}O$ isotopomer photolysis at several different temperatures, 233, 283 and 297 K. (b) Theoretical and experimentally measured isotopic fractionation factors for the $^{14}N^{14}N^{18}O$ isotopomer photolysis at several different temperatures. Experimental values were taken from Griffith *et al.* [5], Johnston *et al.* [6], Kaiser *et al.* [7], Rahn *et al.* [8], Röckmann *et al.* [9], Turatti *et al.* [10]. $T\approx$297 K [5−10].

topic substitution proposed by several workers is still a valid and likely mechanism. However, the change in the cross section for different isotopomers occurs not only because of the shift in the photolysis wavelength but also because of the change in the intensity of the entire absorption line shape. This aspect has not been fully explained in details by previous investigators.

A further cause of fractionation also arises from the complicated topology of the strong angular dependence of the transition dipole moment surfaces, especially in the vicinity of Franck-Condon region. We have seen that the theoretical fractionation produces quite good representation of the experimental fractionation factors for photon energies below 190 nm because the method correctly predicts the increasing or decreasing in the maximum of the absorption cross sections for different isotopomers. Even though the $^{15}N^{14}N^{16}O$ and $^{14}N^{15}N^{16}O$ isotopomers have the same reduced mass, the current wave packet dynamics calculations give two non-identical shapes of cross section, thus making the isotopic fractionation factors of the two isotopomers distinguishable which is in agreement with current mass spectrometric observations. The positive fractionation of the $^{15}N^{14}N^{16}O$ isotopomer between 175 and 188 nm and the largest negative fractionation of the $^{14}N^{15}N^{16}O$ above 195 nm only can be reproduced through the correct treatments of different components in the transition dipole and of angular momentum coupling in the time-dependent formulae [20−22, 24], as has been carried out in the present work. This may be explained by the nature of the initial wavepackets in the Franck-Condon region which is very sensitive to the magnitude of the transition dipoles [15]. Any attempt to change the molecule symmetry as shown by $^{15}N^{14}N^{16}O$ and $^{14}N^{15}N^{16}O$ will lead to considerably different projection of the transition dipole connecting the ground to the upper excited state.

For heavy symmetric molecule such as the $^{14}N^{14}N^{17}O$ and $^{14}N^{14}N^{18}O$ isotopomers, their projections do not differ too much from that of the parent isotopomer and this may explain the averaged fractionations around the maximum absorption are almost zero. On top of that the sharp oscillations are apparent below 180 nm and change the sign of the fractionation factor, thus revealed that the absorption line shape of the oxygen substituted isotopomers are really different from the others. The bound nature of the $2^1A''$ potential [15] allows the N_2-O stretching mode to play greater role in the disso-

DOI:10.1088/1674-0068/24/06/679-685

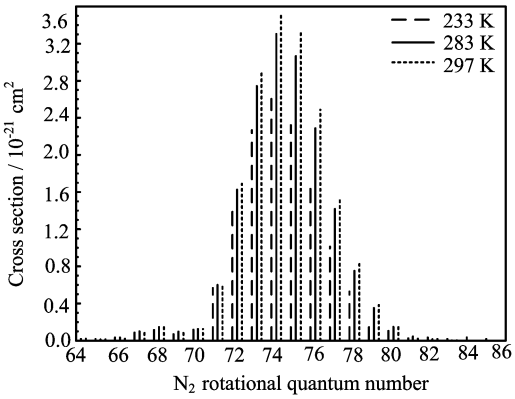

FIG. 5 $^{14}N^{14}N^{16}O$ rotational quantum state distributions at photolysis wavelengths of 203 nm and at temperatures of 233, 283, and 297 K.

ciation process. Any changes in oxygen mass may give rise to a different shape of the spectrum and definitely, to a different trend of the isotopic fractionation factor.

Figures 1−4 display that the temperature effects on the isotopic fractionation are weaker at high energy tail. Our findings predict that for the nitrogen substituted isotopomers (see Figs.1−3), higher fractionation is induced by lowering the temperature which is in qualitative agreement with experimental observations by Kaiser *et al.* [7]. However, this trend is reversed for the isotopomers with heavy oxygen substituted. Hot bands are certainly involved in the temperature dependence of the N_2O spectrum namely its role is expected to be confined to the blue or red side of the spectral maximum. The actual isotopic fractionation of N_2O relies on the solar ultraviolet window, and accordingly on altitude. The current findings provide a reliable model for predicting the trend of isotopic fractionation in the stratosphere at different latitudes. Largest fractionation of nitrogen substituted isotopomers may occur in the low-altitude stratosphere, since stratosphere temperature increases gradually with height. Conversely, the fractionation factor for the oxygen substituted isotopomers increases with decreasing altitude.

B. Product rotational quantum state distributions

Figures 5−7 display the rotational quantum state distribution for the $^{14}N^{14}N^{16}O$, $^{14}N^{15}N^{16}O$, $^{15}N^{14}N^{16}O$, $^{15}N^{15}N^{16}O$, $^{14}N^{14}N^{17}O$, and $^{14}N^{14}N^{18}O$ isotopomers computed from the contribution of three lowest excited states, $2^1A'$, $1^1A''$ and $2^1A''$. Each of the rotational quantum state distributions is obtained by Boltzmann averaging of three cross sections with the N_2O molecules initially in its (0,0,0), (0,1,0), (0,2,0), and (1,0,0) vibrational states.

The N_2 distribution for the $^{14}N^{14}N^{16}O$ isotopomer peaks at j=74 which is in excellent agreement with the experimentally observed distribution for photolysis at

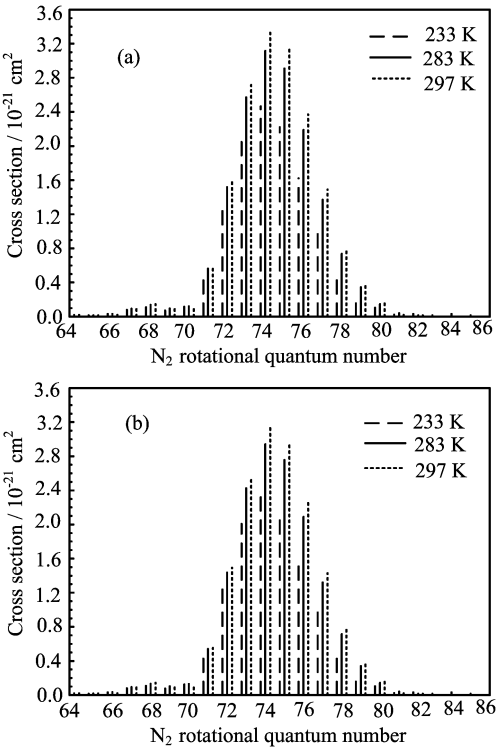

FIG. 6 Isotopically oxygen substituted N_2O rotational quantum state distributions at photolysis wavelength of 203 nm and at temperatures of 233, 283, and 297 K. (a) $^{14}N^{14}N^{17}O$ and (b) $^{14}N^{14}N^{18}O$.

203 nm [33]. Our trend of hot rotational excitation is enhanced by (0,1,0) bending vibration as has been observed by Kawamata *et al.* [33]. The largest portion of the rotationally hot N_2 originates primarily from excitation to the $2^1A'$ state. The strongly repulsive nature of the $2^1A'$ potential energy surface along the N_2-O coordinate is consistent with the large positive anisotropy parameter observed by Neyer *et al.* [34, 35]. We believe that a strong perpendicular contribution to the photodissociation reflects the significant y component of the transition dipole moment which is perpendicular to the N_2-O dissociation direction.

For oxygen substituted N_2O, they display a strong peak at j=74 which is identical with the $^{14}N^{14}N^{16}O$ isotopomer, revealing that there is only a minor change in the distribution. This is not surprising due to fact that both the heavy isotopomers produce the same $^{14}N^{14}N$ photofragments as the parent one. For nitrogen-substituted N_2O, their distributions tend to be shifted to higher rotational states due to the larger moment of inertia of the $^{14}N^{15}N$ and $^{15}N^{15}N$ photofragments which generate a strong torque around the center of mass of N_2O molecule. Relative to the maximum peak of the $^{14}N^{14}N^{16}O$ distribution, the maximum peak of the $^{14}N^{15}N^{16}O$ is shifted to j=75, of the $^{15}N^{14}N^{16}O$ to j=76, and of the $^{15}N^{15}N^{16}O$ to j=77. Same as its fractionation factors, the distributions of $^{14}N^{15}N^{16}O$

DOI:10.1088/1674-0068/24/06/679-685

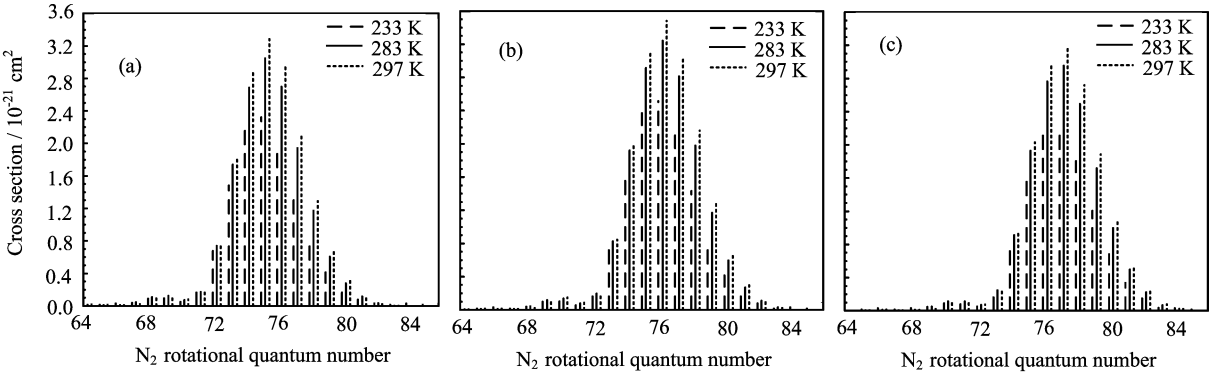

FIG. 7 Isotopically nitrogen substituted of N_2O rotational quantum state distributions at photolysis wavelength of 203 nm and at temperatures of 233, 283 and 297 K. (a) $^{14}N^{15}N^{16}O$, (b) $^{15}N^{14}N^{16}O$, and (c) $^{15}N^{15}N^{16}O$.

and $^{15}N^{14}N^{16}O$ isotopomers are distinguishable as well by one unit angular momentum at its maximum peak, presenting an interesting opportunity for future atmospheric modeling of N_2O. This trend of the distributions are not clearly observed and well explained in the calculations by Nanbu and Johnson [19] who may have concentrated their work more on absorption cross sections.

The influence of different temperatures (233, 283, and 297 K) on the rotational quantum state distributions for six isotopomers is illustrated in Figs. 5−7. It is clear that with increasing temperature, the intensity of the N_2 product distribution increases, most significantly around the maximum peak of the distribution.

IV. CONCLUSION

The time-dependent quantum wave packet method has correctly predicted the sign of the isotopic fractionation factors of N_2O isotopomers observed experimentally. The method also predicted an observable difference in $^{14}N^{15}N^{16}O/^{15}N^{14}N^{16}O$ fractionation factors and the rotational distribution of N_2. A detailed explanation of the shifting in the wavelength-dependent absorption spectra and in the product state distributions has been addressed in the present work.

Accurate isotopic fractionation determinations depend on the quality of the global topology of both the ground and excited electronic states, the transition dipole moment function and the energy separation between the potentials. Small inaccuracies in any of these components may lead to imprecise results. In this regard, our previous computed potential energy and transition dipole moment surfaces have been tested for their reliability and accuracy in that all the calculated isotopic fractionation factors of heavy isotopomers agree almost quantitatively with several experimentally derived results.

We have shown that the inclusion of the $2^1A''$ state in the calculation has considerably reproduced some of the experimental diffuse structures in the spectrum. Thus, we strongly suggest that it is necessary to take into account the non-adiabatic effect of Renner-Teller coupling between $2^1A''$ and $2^1A'$ states in order to obtain a complete representation of theoretical absorption spectrum around the maximum peak. The coupling perhaps would allow some of N_2O molecules in the $2^1A'$ state crossing over to the $2^1A''$ state and trap in the $2^1A''$ potential well. Such consideration would require more computational facilities and time than that was used here. This aspect will be considered in our future work.

V. ACKNOWLEDGMENT

This work was supported by the research grant of the University of Malaya.

[1] R. P. Wayne, *Chemistry of Atmospheres*, Oxford: Clarendon Press, (1991).
[2] P. Crutzen, J. Geophys. Res. **76**, 7311 (1971).
[3] K. Minschwaner, R. Salawitch, and M. McElroy, J. Geophys. Res. **98**, 10543 (1993).
[4] S. Cliff, C. Brenninkmeijer, and M. Thiemens, J. Geophys. Res. **104**, 16171 (1999).
[5] D. W. T. Griffith, G. C. Toon, B. Sen, J. F. Blavier, and R. A. Toth, Geophys. Res. Lett. **27**, 2485 (2000).
[6] J. Johnston, S. Cliff, and M. Thiemens, J. Geophys. Res. **100**, 16801 (1995).
[7] J. Kaiser, T. Röckmann, C. A. M. Brenninkmeijer, and P. J. Crutzen, Atmos. Chem. Phys. **3**, 303 (2003).
[8] T. Rahn, H. Zhang, M. Wahlen, and G. A. Blake, Geophys. Res. Lett. **25**, 4489 (1998).
[9] T. Röckmann, C. A. M. Brenninkmeijer, M. Wollenhaupt, J. N. Crowley, and P. J. Crutzen, Geophys. Res. Lett. **27**, 1399 (2000).
[10] F. Turatti, D. W. T. Griffith, S. R. Wilson, M. B. Esler, T. Rahn, H. Zhang, and G. A. Blake, Geophys. Res. Lett. **27**, 2489 (2000).

DOI:10.1088/1674-0068/24/06/679-685

[11] P. von Hessberg, J. Kaiser, M. B. Enghoff, C. A. McLinden, S. L. Sorensen, T. Röckmann, and M. S. Johnson, Atmos. Chem. Phys. **4**, 1237 (2004).
[12] H. Zhang, P. O. Wennberg, V. H. Wu, and G. A. Blake, Geophys. Res. Lett. **27**, 2481 (2000).
[13] Y. L. Yung and C. E. Miller, Science **278**, 1778 (1997).
[14] A. Brown, P. Jimeno, and G. G. Balint-Kurti, J. Phys. Chem. A **103**, 11089 (1999).
[15] M. N. Daud, G. G. Balint-Kurti, and A. Brown, J. Chem. Phys. **122**, 054305 (2005).
[16] D. G. Hopper, J. Chem. Phys. **80**, 4290 (1984).
[17] M. S. Johnson, G. D. Billing, A. Gruodis, and M. H. M. Janssen, J. Phys. Chem. A **105**, 8672 (2001).
[18] K. P. Meher, D. W. Jason, and R. A. Marcus, J. Geophys. Res. **110**, D21315 (2005).
[19] S. Nanbu and M. S. Johnson, J. Phys. Chem. A **108**, 8905 (2004).
[20] G. G. Balint-Kurti, Adv. Chem. Phys. **128**, 249 (2004).
[21] G. G. Balint-Kurti and A. Brown, *Theory of Chemical Reaction Dynamics*, The Netherlands: Kluwer Academic Publishers, 149 (2004).
[22] G. G. Balint-Kurti, L. Füsti-Molnár, and A. Brown, Phys. Chem. Chem. Phys. **3**, 702 (2001).
[23] E. J. Heller, J. Chem. Phys. **68**, 2066 (1978).
[24] M. N. Daud and G. G. Balint-Kurti, Chin. Phys. Lett. **26**, 073302 (2009).
[25] G. G. Balint-Kurti, R. N. Dixon, and C. C. Marston, J. Chem. Soc. Faraday Trans. **86**, 1741 (1990).
[26] Á. Vibók and G. G. Balint-Kurti, J. Chem. Phys. **96**, 7615 (1992).
[27] Á. Vibók and G. G. Balint-Kurti, J. Phys. Chem. **96**, 8712 (1992).
[28] G. S. Selwyn, J. Podolske, and H. S. Johnston, Geophys. Res. Lett. **4**, 427 (1977).
[29] W. B. De More, S. P. Sander, C. J. Howard, A. R. Ravishankara, D. M. Golden, C. E. Kolb, R. F. Hampson, M. J. Kurylo, and M. J. Molina, *Chemical Kinetics and Photochemical Data for Use in Stratospheric Modeling*, Evaluation Number 12, JPL Publication 97-4, Pasadena: Jet Propulsion Laboratory, California Institute of Technology, (1997).
[30] M. F. Ḿerienne, B. Coquart, and A. Jenouvrier, Planet. Space Sci. **38**, 617 (1990).
[31] K. Yoshino, D. E. Freeman, and W. H. Parkinson, Planet. Space Sci. **32**, 1219 (1984).
[32] G. S. Selwyn and H. S. Johnston, J. Chem. Phys. **74**, 3791 (1981).
[33] H. Kawamata, H. Kohguchi, T. Nishide, and T. Suzuki, J. Chem. Phys. **125**, 133312 (2006).
[34] D. W. Neyer, A. J. R. Heck, and D. W. Chandler, J. Chem. Phys. **110**, 3411 (1999).
[35] D. W. Neyer, A. J. R. Heck, D. W. Chandler, J. M. Teule, and M. H. M. Janssen, J. Phys. Chem. A **103**, 10388 (1999).

DOI:10.1088/1674-0068/24/06/679-685